

Topological bulk and edge correlations of BCS condensate in a two-dimensional singlet-triplet spin pairing model

E. S. Ma, K. L. Zhang,^{*} and Z. Song[†]
School of Physics, Nankai University, Tianjin 300071, China

The condensate of the Bardeen-Cooper-Schrieffer (BCS) pair in the ground state, which may contain information on both topology and spin pairing, promises the superconductivity of the system. In this paper, we study a singlet-triplet spin pairing model on a square lattice and investigate the consequences of the competition of on-site and nearest neighbor pairing parameters. We show that the ground state of the system has the form of the condensate of the BCS pair, and the topological transition is associated with the nonanalytic behavior of the pairing order parameters. A real space correlation function on opposite spin direction is introduced to characterizing the topological phase of the many-body ground state. Numerical results demonstrate that this method works well in the presence of disordered perturbation, lattice defects, or irregular boundary conditions. The real space correlation function between two edges of the system is also discussed, which directly reflects the existence of topological edge modes in the many-body ground state.

I. INTRODUCTION

The topological phase of matter has received much attention in recent decades due to its robust physical properties, which offer potential applications for novel devices and quantum information technology [1–16]. From the perspective of topological band theory, these phases fall into two categories [17]: fully gapped topological phases, such as topological insulators and topological superconductors [9, 10, 18], and gapless topological phases, such as topological semimetals and nodal superconductors [12, 13, 19–26]. The common characteristic of these topological matters is the existence of topological protected edge modes. Unlike topological insulators (semimetals), the edge modes of topological (nodal) superconductors neither particles nor holes but Bogoliubov quasiparticles, which provide a superconducting channel at the boundary. In terms of the classification of superconducting pairing about spin structures, the Cooper pairs may contain singlet or triplet pairing components, which is frequently discussed in the realm of superconductivity [27–31].

The existence of topological protected edge modes can be predicted by the bulk topological invariants constructed from the bulk Hamiltonian in momentum space, which is referred to as bulk-boundary correspondence (BBC) [32–36] and is of fundamental importance in studies of the topological phase of matter. In recent years, more efforts have been made to develop real-space characterization methods for topological phases, for example, real-space topological markers constructed from projectors and position operators [37–40] and approaches based on correlation functions [41, 42] or entanglement spectra [43–45]. The main advantage of these methods is that they are more relevant to real systems in experiments, i.e., for systems without translation symmetry, examples

of which include systems with defects or disorder [37, 40]. The topological Anderson insulator predicted and discovered in recent years [46–48] is another well-known example for the role of real-space characterization methods. Most recently, theoretical proposal suggests that some topological markers may be measured by real-space experiments [39].

In this paper, we study a mixed singlet-triplet spin pairing model on a square lattice, the Hamiltonian of which is quadratic and includes pairing terms, i.e., on-site pairing and nearest neighbor pairing between opposite spin directions. We investigate the consequences of the competition of different pairing parameters. It shows that the ground state of the system has the form of the condensate of the Bardeen-Cooper-Schrieffer (BCS) [49] pair. To characterize the phase transition and the properties of the ground state, we introduce the pairing order parameter and find that the topological transition is associated with the nonanalytic behavior of the order parameter. Furthermore, we find that the phase factor in the ground state related to the system topology can be revealed by a real space correlation function in the opposite spin direction, which provides a real-space scheme for detecting the topological phase of a class of systems. Numerical results demonstrate that this method works well in the presence of disordered perturbation, random lattice defects, or when irregular boundary conditions are adopted. Besides, we also compute the real space correlation function between two edges of the system, which directly reflects the existence of topological edge modes in the many-body ground state, verifying the BBC from the perspective of real space bulk and edge correlation functions.

This paper is organized as follows. In Sec. II, we introduce the model, reveal the topological phase diagram, and show that the ground state has the form of the condensate of the BCS pair. In Sec. III, we investigate the real space bulk and edge correlation functions of the many-body ground state of the system. Finally, we summarize and discuss the results of the paper in Sec. IV.

^{*} zkl@mail.nankai.edu.cn

[†] songtc@nankai.edu.cn

II. MODEL AND PHASE DIAGRAM

First, we consider a mixed singlet-triplet spin pairing model defined on a square lattice, the Hamiltonian of which has the form

$$H = \sum_{\mathbf{r}} \sum_{\mathbf{a}=\hat{x},\hat{y}} (\Delta_+ c_{\mathbf{r},\downarrow} c_{\mathbf{r}+\mathbf{a},\uparrow} + \Delta_- c_{\mathbf{r}+\mathbf{a},\downarrow} c_{\mathbf{r},\uparrow}) + \Delta_0 \sum_{\mathbf{r}} c_{\mathbf{r},\downarrow} c_{\mathbf{r},\uparrow} + \text{H.c.}, \quad (1)$$

where Δ_0 and Δ_{\pm} are real parameters for on-site and nearest neighbor pairings, respectively. The index $\mathbf{r} = (m, n)$ denotes the lattice coordinate; \hat{x} and \hat{y} are unit vectors in the x and y directions. Different from most related works, the Hamiltonian in Eq. (1) only contains the pairing terms, and we are interested in the consequence of the competition between the on-site and nearest neighbor pairings.

Employing the periodic boundary conditions in both directions and applying the Fourier transformation

$$c_{\mathbf{k},\sigma} = \sum_{\mathbf{r}} e^{i\mathbf{k}\cdot\mathbf{r}} c_{\mathbf{r},\sigma}, \quad (2)$$

we obtain the Hamiltonian in \mathbf{k} space

$$H = \sum_{\mathbf{k}} C_{\mathbf{k}}^{\dagger} H_{\text{BdG}}(\mathbf{k}) C_{\mathbf{k}}, \quad (3)$$

where the Nambu spinor is defined as $C_{\mathbf{k}}^{\dagger} = (c_{\mathbf{k},\uparrow}^{\dagger} \ c_{-\mathbf{k},\downarrow} \ c_{\mathbf{k},\downarrow}^{\dagger} \ c_{-\mathbf{k},\uparrow})$. The Bogoliubov-de-Gennes (BdG) representation of the Hamiltonian is a block diagonal matrix:

$$H_{\text{BdG}}(\mathbf{k}) = \frac{1}{2} \begin{pmatrix} H(\mathbf{k}) & \mathbf{0} \\ \mathbf{0} & -H(-\mathbf{k}) \end{pmatrix}, \quad (4)$$

where $H(\mathbf{k})$ represents a pseudo spin Hamiltonian $H(\mathbf{k}) = B_x(\mathbf{k})\sigma_x + B_y(\mathbf{k})\sigma_y$ in the effective magnetic field

$$\begin{aligned} B_x(\mathbf{k}) &= (\Delta_+ + \Delta_-)(\cos k_x + \cos k_y) + \Delta_0, \\ B_y(\mathbf{k}) &= (\Delta_+ - \Delta_-)(\sin k_x + \sin k_y). \end{aligned} \quad (5)$$

In fact, Hamiltonian $H(\mathbf{k})$ can be related to a spinless Kitaev model by the unitary transformation $c_{\mathbf{k},\uparrow} = (c_{\mathbf{k}} - c_{-\mathbf{k}}^{\dagger})/\sqrt{2}$, $c_{-\mathbf{k},\downarrow}^{\dagger} = (c_{\mathbf{k}} + c_{-\mathbf{k}}^{\dagger})/\sqrt{2}$. In this sense, $c_{\mathbf{k},\uparrow}$ and $c_{-\mathbf{k},\downarrow}^{\dagger}$ are pseudo-spin operators.

The real functions $B_x(\mathbf{k})$ and $B_y(\mathbf{k})$ are the coefficients of singlet and triplet pairing in momentum space. The Fermi statistics place constraints on the forms of functions $B_x(\mathbf{k})$ and $B_y(\mathbf{k})$. For example, we take the singlet term,

$$\begin{aligned} & \sum_{\mathbf{k}} [B_x(\mathbf{k})(c_{\mathbf{k},\uparrow}^{\dagger} c_{-\mathbf{k},\downarrow}^{\dagger} - c_{\mathbf{k},\downarrow}^{\dagger} c_{-\mathbf{k},\uparrow}^{\dagger}) \\ &= \sum_{\mathbf{k}} [B_x(-\mathbf{k})(-c_{\mathbf{k},\downarrow}^{\dagger} c_{-\mathbf{k},\uparrow}^{\dagger} + c_{\mathbf{k},\uparrow}^{\dagger} c_{-\mathbf{k},\downarrow}^{\dagger}), \end{aligned} \quad (6)$$

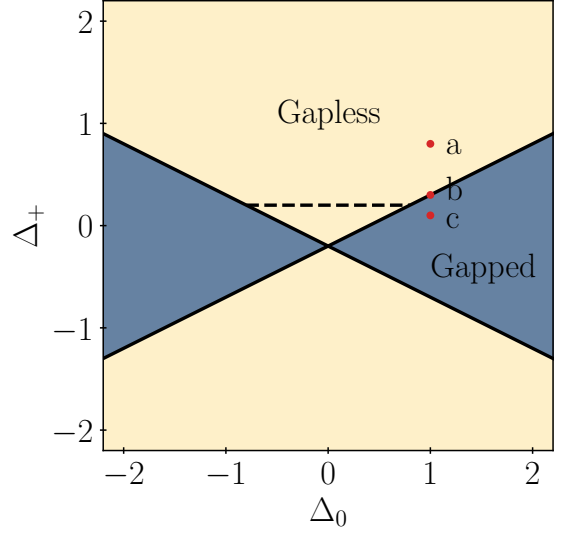


FIG. 1. Phase diagram in the Δ_0 - Δ_+ parameter plane for the model studied in this paper. The black lines indicate the phase boundary that separates the topological trivial (gapped; gray region) and nontrivial (gapless; yellow region) phases identified by the winding number of the vector field $\hat{\mathbf{B}}$ or the order parameter O of the ground state. The dashed line represents the parameter $\Delta_+ = \Delta_-$, where the system is trivial. The other parameter is set as $\Delta_- = 0.2$. The three red dots correspond to the parameters of the systems taken in the numerical computations for Figs. 3 (a)-(c).

so that $B_x(\mathbf{k}) = B_x(-\mathbf{k})$. Similarly, we have $B_y(\mathbf{k}) = -B_y(-\mathbf{k})$ for the triplet term. This constraint can also be given by the particle-hole symmetry of the BdG Hamiltonian, that is $H_{\text{BdG}}(\mathbf{k}) = -\mathcal{C}H_{\text{BdG}}(-\mathbf{k})\mathcal{C}^{-1}$, where $\mathcal{C} = \sigma_x \otimes \sigma_x \mathcal{K}$ and \mathcal{K} is the complex-conjugation operator. The model also obeys time reversal and inversion symmetry, i.e., for the BdG Hamiltonian we have $H_{\text{BdG}}(\mathbf{k}) = \mathcal{T}H_{\text{BdG}}(-\mathbf{k})\mathcal{T}^{-1}$ and $H_{\text{BdG}}(\mathbf{k}) = \mathcal{P}H_{\text{BdG}}(-\mathbf{k})\mathcal{P}^{-1}$, with $\mathcal{T} = \mathcal{K}$ and $\mathcal{P} = \sigma_0 \otimes \sigma_x$; σ_0 is a 2×2 identity matrix.

By diagonalizing the Hamiltonian H in Eq. (3), the ground state is obtained as

$$|G\rangle = \prod_{\mathbf{k}} \frac{1 + e^{i\phi_{\mathbf{k}}} c_{-\mathbf{k},\downarrow}^{\dagger} c_{\mathbf{k},\uparrow}^{\dagger}}{\sqrt{2}} |0\rangle, \quad (7)$$

where the angle is

$$\phi_{\mathbf{k}} = \arg(B_x - iB_y). \quad (8)$$

Note that the ground state can be rewritten in the form

$$|G\rangle = \sum_{n=0}^{N^2} \frac{2^{-N^2/2}}{n!} (s^+)^n |0\rangle. \quad (9)$$

Unlike the conventional BCS wave function, the ground state in Eq. (9) describes the condensate of the BCS pair.

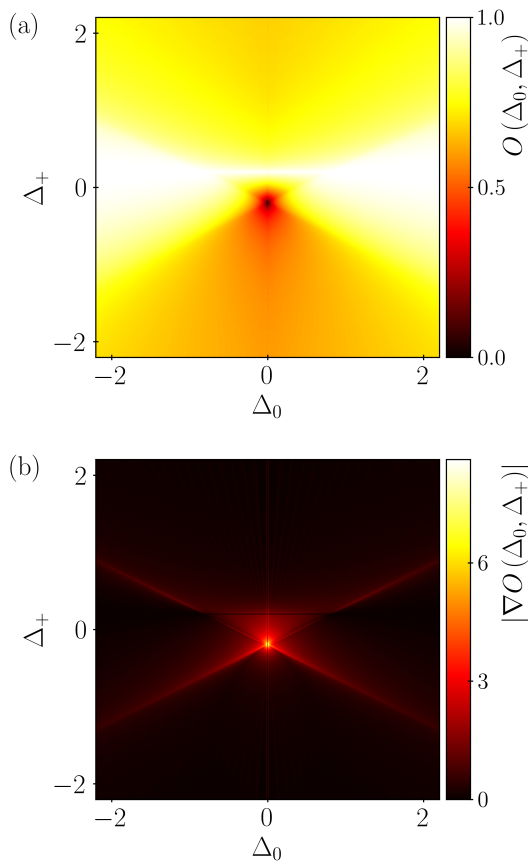


FIG. 2. Numerical results of the order parameter. (a) The pairing order parameter O in Eq. (14) in the Δ_0 - Δ_+ parameter plane. (b) The corresponding absolute value of the gradient of the order parameter O in the Δ_0 - Δ_+ plane, which indicates the phase boundary. Other parameters are set as $\Delta_- = 0.2$ and $N = 100$.

The operators

$$s^+ = (s^-)^\dagger = \sum_{\mathbf{k}} e^{i\phi_{\mathbf{k}}} c_{-\mathbf{k},\downarrow}^\dagger c_{\mathbf{k},\uparrow}^\dagger,$$

$$s^z = \frac{1}{2} \sum_{\mathbf{k}} \left(c_{\mathbf{k},\uparrow}^\dagger c_{\mathbf{k},\uparrow} + c_{-\mathbf{k},\downarrow}^\dagger c_{-\mathbf{k},\downarrow} - 1 \right), \quad (10)$$

are pseudo-spin operators that satisfy the Lie algebra commutation relation $[s^z, s^\pm] = \pm s^\pm$.

We note that the angle $\phi_{\mathbf{k}_c}$ is ill-defined at the zero point of $|\mathbf{B}|$ with

$$B_x(\mathbf{k}_c) = B_y(\mathbf{k}_c) = 0, \quad (11)$$

which corresponds to the topological defect of the vector field $\hat{\mathbf{B}} = (\cos \phi_{\mathbf{k}}, \sin \phi_{\mathbf{k}})$ if the solutions of $\mathbf{k}_c = (k_{xc}, k_{yc})$ are isolated points in the \mathbf{k} -plane. In this sense, the condensate of the collective BCS-pair state $s^+ |0\rangle$ is topologically nontrivial and is characterized by the vortex of field $\hat{\mathbf{B}}$. Obviously, such a ground state is a gapless

state. In fact, when $\Delta_+ \neq \Delta_-$, we have

$$k_{xc} = -k_{yc} = \pm \arccos \left[-\frac{\Delta_0}{2(\Delta_+ + \Delta_-)} \right], \quad (12)$$

in the topological nontrivial region $|\Delta_0| < 2|\Delta_+ + \Delta_-|$ ($\Delta_+ \neq \Delta_-$). The two zero points (k_{xc}, k_{yc}) and $(-k_{xc}, -k_{yc})$ are Dirac points in momentum space, the topological nature of which are characterized by the winding number [12, 50–52] of the vortex in the vector field $\hat{\mathbf{B}}$. The combination of the time reversal and inversion symmetry protects the Dirac points in the following sense: the diagonal term in $H_{\text{BdG}}(\mathbf{k})$ that openings a gap is forbidden by time reversal and inversion symmetry. The position of the Dirac points only shifts when changing the system parameters until the Dirac points merge and open a gap when $|\Delta_0| \geq 2|\Delta_+ + \Delta_-|$. The phase diagram of the system is presented in Fig. 1. In the next section, we will show that the vector field $\hat{\mathbf{B}}$ can be extracted from the real space correlation function of the ground state, where the periodic boundary condition is no longer needed.

To characterize the phase transition and the properties of the ground state, we introduce the following pairing order parameter

$$O = \frac{1}{N^2} \sum_{\mathbf{k}} \left| \langle G | c_{\mathbf{k},\uparrow}^\dagger c_{-\mathbf{k},\downarrow}^\dagger + c_{-\mathbf{k},\downarrow} c_{\mathbf{k},\uparrow} | G \rangle \right|. \quad (13)$$

Direct calculation shows that

$$O = \frac{1}{N^2} \sum_{\mathbf{k}} |\cos \phi_{\mathbf{k}}|, \quad (14)$$

which characterizes the pairing channel in \mathbf{k} space, and is related to the angle $\phi_{\mathbf{k}}$ in the vector field $\hat{\mathbf{B}}$ that contains information of the system topology.

In Fig. 2 (a), we plot the numerical results of the order parameter O in the Δ_0 - Δ_+ parameter plane. We can see that in the gapped phase, the \mathbf{k} -space pairing strength is stronger than that in the gapless phase. The absolute value of the gradient of the order parameter O presented in Fig. 2 (b) indicates that topological phase transition is associated with the nonanalytic behavior of the order parameter O .

III. BULK-BOUNDARY CORRESPONDENCE BY REAL SPACE CORRELATION

In the previous section, we have shown that the order parameter O is related to the angle $\phi_{\mathbf{k}}$ in the vector field $\hat{\mathbf{B}}$, which contains information on the system topology. Therefore, it is promising to extract the topological properties of the system from a specific correlation function, preferably the real space correlation function. To

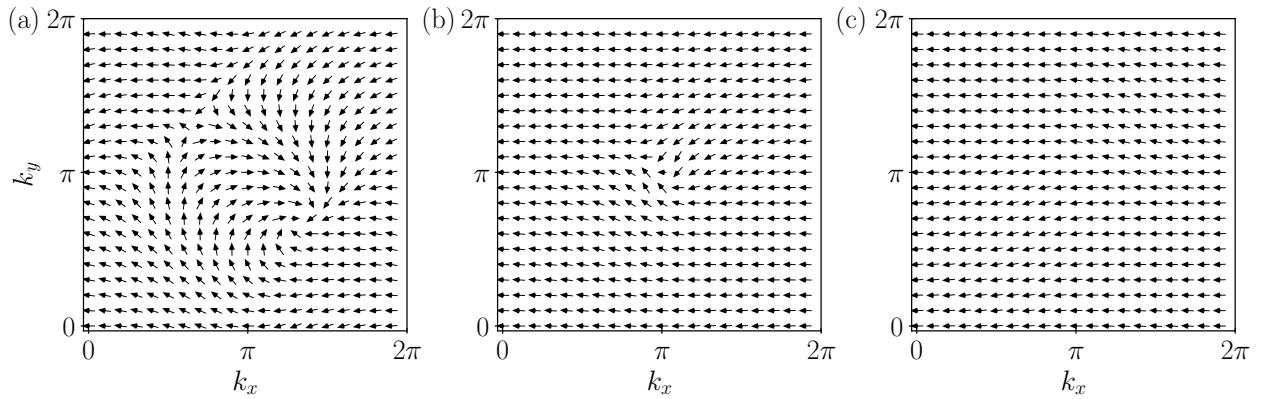


FIG. 3. Plots of the numerical results of the phase angle $\phi_{\mathbf{k}}$ computed from the real space correlation function $\mathcal{C}_{\mathbf{r}}$ in Eq. (16). The direction of the arrow at different \mathbf{k} represents the phase angle $\phi_{\mathbf{k}}$. The system parameters taken are marked by the red dots in the phase diagram of Fig. 1: (a) topological nontrivial case $\Delta_+ = 0.8$; (b) critical case $\Delta_+ = 0.3$; and (c) topological trivial case $\Delta_+ = 0.1$. Other parameters are taken as $N = 20$, $\Delta_0 = 1$ and $\Delta_- = 0.2$. The open boundary condition in both directions of the square lattice is taken.

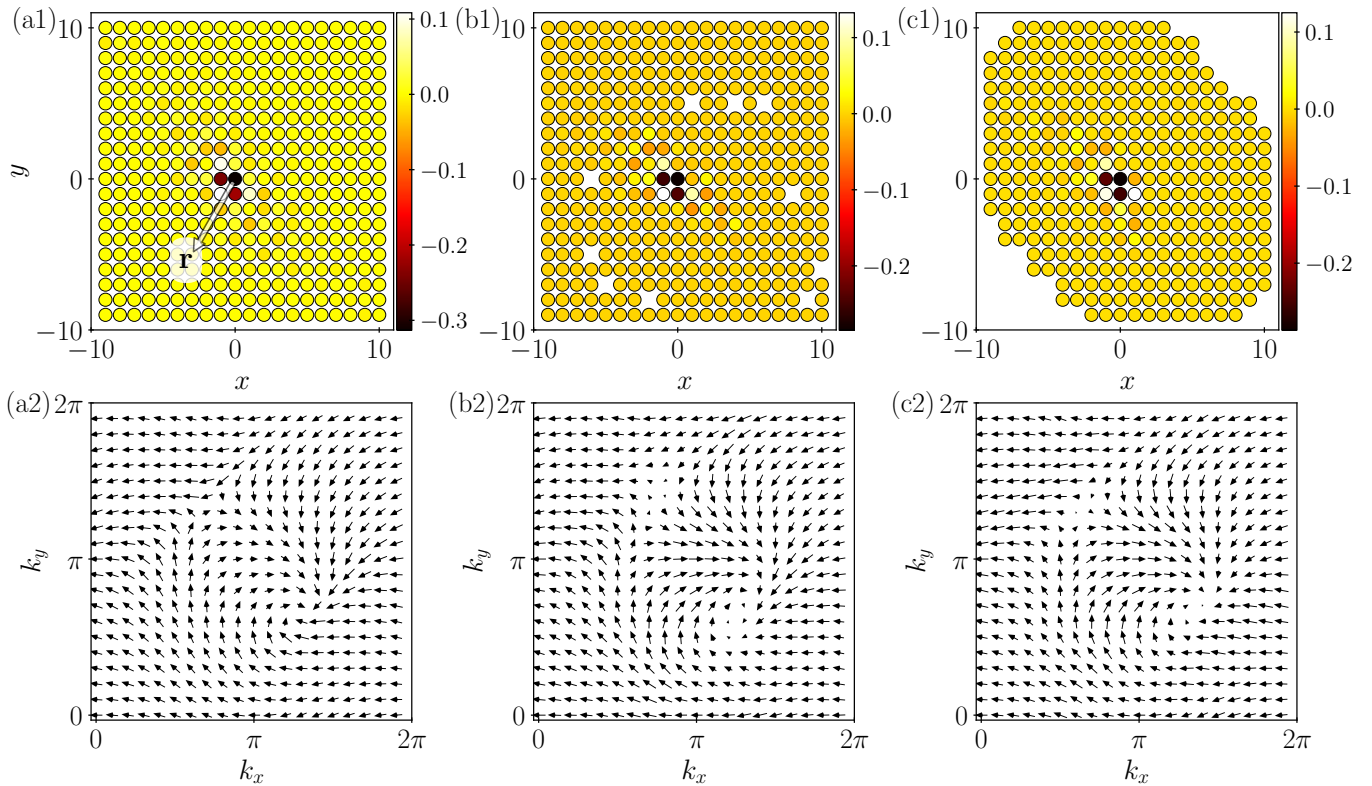


FIG. 4. Numerical results of the real space correlation function $\mathcal{C}_{\mathbf{r}}$ and phase angle $\phi_{\mathbf{k}}$ in the presence of (a) disordered perturbation, where the system parameters are nonuniform in space and each deviates a uniform distributed random real number within the interval $[-0.2, 0.2]$; (b) random defects, where the spatial coordinates of 10 lattice defects are randomly taken; and (c) irregular boundary as shown in (c1). The system parameters are taken as $\Delta_+ = 0.8$, $\Delta_- = 0.2$ and $\Delta_0 = 1$.

this end, we consider the following correlation function in real space

$$\mathcal{C}_{\mathbf{r}} = \langle G | c_{\mathbf{0},\uparrow} c_{\mathbf{r},\downarrow} | G \rangle, \quad (15)$$

where the coordinate origin $\mathbf{0}$ is placed in the center of the lattice when the open boundary condition is adopted.

The correlation function $\mathcal{C}_{\mathbf{r}}$ and the phase $e^{-i\phi_{\mathbf{k}}}$ in the ground state are related by the Fourier transformation

$$e^{i\phi_{\mathbf{k}}} = 2 \sum_{\mathbf{r}} e^{i\mathbf{k}\cdot\mathbf{r}} \mathcal{C}_{\mathbf{r}}. \quad (16)$$

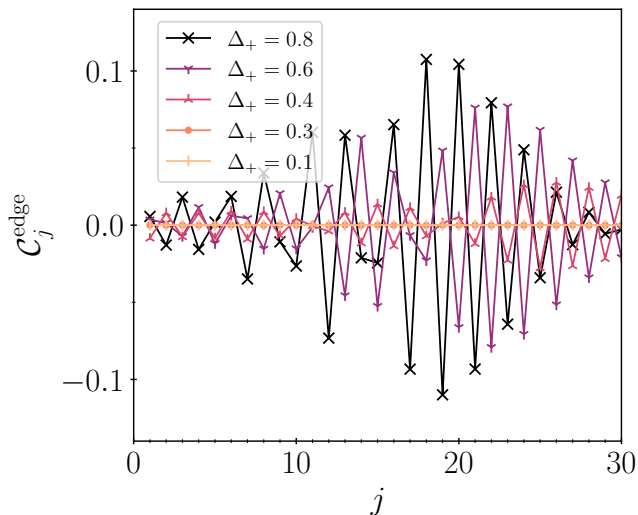


FIG. 5. Numerical results of the edge correlation function defined in Eq. (18) for the topological nontrivial phase $\Delta_+ > 0.3$, critical point $\Delta_+ = 0.3$ and topological trivial phase $\Delta_+ = 0.1$. Other system parameters are set as $N = 30$, $\Delta_0 = 1$ and $\Delta_- = 0.2$. The cylindrical boundary condition for the square lattice is taken.

In fact, from the definition of the correlation function and taking the form of the ground state $|G\rangle$ in Eq. (7) into account, we have

$$\begin{aligned}
 C_{\mathbf{r}} &= \frac{1}{N^2} \sum_{\mathbf{k}, \mathbf{k}'} e^{i\mathbf{k}' \cdot \mathbf{r}} \langle G | c_{\mathbf{k}, \uparrow} c_{\mathbf{k}', \downarrow} | G \rangle \\
 &= \frac{1}{N^2} \sum_{\mathbf{k}} e^{-i\mathbf{k} \cdot \mathbf{r}} \langle G | c_{\mathbf{k}, \uparrow} c_{-\mathbf{k}, \downarrow} | G \rangle \\
 &= \frac{1}{2N^2} \sum_{\mathbf{k}} e^{i\phi_{\mathbf{k}}} e^{-i\mathbf{k} \cdot \mathbf{r}}.
 \end{aligned} \tag{17}$$

Thus, we have the relation in Eq. (16) by the Fourier transformation. This inspires us to employ the real space correlation function $C_{\mathbf{r}}$ for detecting the topological properties of the ground state. Different from the topological invariant defined in momentum space, this method is applicable for systems without translation symmetry, including systems with disorder and defects. In the following, we present the numerical results to demonstrate our conclusions. Numerically, the real space correlation function for the ground state of a quadratic Hamiltonian can be computed by the method presented in Appendix A.

First, we compute the real space correlation function $C_{\mathbf{r}}$ defined in Eq. (15). The open boundary condition in both directions of the lattice is taken. Although the derivation of the relation between $C_{\mathbf{r}}$ and the phase $e^{-i\phi_{\mathbf{k}}}$ in Eq. (16) requires periodic boundary condition, it is expected that if $C_{\mathbf{r}}$ decays rapidly with the distance between $\mathbf{0}$ and \mathbf{r} (which is examined by the subsequent numerical calculations), then the phase $e^{-i\phi_{\mathbf{k}}}$ is almost unaffected by the boundary conditions. Then, we are allowed to

compute the phase $e^{-i\phi_{\mathbf{k}}}$ through Eq. (16) for each \mathbf{k} . We present the numerical results in Fig. 3, in which the phase angle $\phi_{\mathbf{k}}$ is denoted by the direction of the arrow at \mathbf{k} . The results indicate that the phase angle can be correctly obtained from the real space correlation function $C_{\mathbf{r}}$: we can see that two vortices emerge in the topological nontrivial case [Fig. 3 (a)] and then merge and vanish in the critical and topological trivial cases [Figs. 3 (b) and (c)] when system parameter Δ_+ varies.

Furthermore, numerical simulations show that the topological feature is robust in the presence of (a) disordered perturbation, (b) random defects and (c) irregular boundaries. In Fig. 4, we present the lattice geometries, the numerical results of the real space correlation function $C_{\mathbf{r}}$, and the phase angle $\phi_{\mathbf{k}}$ for these three cases. In Fig. 4 (a), the system parameters Δ_+ , Δ_- and Δ_0 are nonuniform in space, and each deviates a uniform distributed random real number within the interval $[-0.2, 0.2]$. The result in Fig. 4 (a1) indicates that the correlation function $C_{\mathbf{r}}$ decays rapidly with the distance between $\mathbf{0}$ and \mathbf{r} . In comparison with Fig. 3 (a), the result in Fig. 4 (a2) shows that the pattern of the vortices is robust against disordered perturbation. Fig. 4 (b) shows the numerical results for the lattice with random defects, where the spatial coordinates of 10 lattice defects are randomly taken. Fig. 4 (c) shows the numerical results for the lattice with irregular boundaries. We can see that the signatures of the vortices are also robust for these two cases.

Now, we turn to the investigation on the relation between the bulk topology and edge correlation. It can be shown that in the topological nontrivial phase, the Majorana zero modes appear at the boundaries of the system (see Appendix B). The zero modes may contribute to the correlation function between two edges of the system [53, 54], which is one of the signatures of the system topology. To verify this point for our model, we introduce the following edge correlation function:

$$C_j^{\text{edge}} = \langle G | c_{(1,1), \uparrow} c_{(N,j), \downarrow} | G \rangle, \tag{18}$$

where $|G\rangle$ is the ground state of the system under cylindrical boundary conditions; $(1, 1)$ and (N, j) are the lattice coordinates of the two ends of the system, and j is the lattice coordinate along one of the edges of the lattice cylinder. In Fig. 5, we present the numerical results of the edge correlation functions for the systems in different phases with different parameter Δ_+ . This indicates that the edge correlation function is nonzero in the topological nontrivial phase but vanishes in the trivial phase. Therefore, we conclude that the edge correlation function can reflect the phase diagram in Fig. 1.

The above numerical results of the bulk correlation function and the edge correlation function in different phases verify the BBC from another perspective, in contrast with the relation between the topological invariant and single-particle edge mode.

IV. SUMMARY AND DISCUSSION

In summary, we have investigated a mixed singlet-triplet spin pairing model on a square lattice. The ground state of the system has the form of the condensate of BCS pairs, and in the gapless phase, topological edge modes emerge when the open boundary condition is adopted. The topological transition is associated with the nonanalytic behavior of the order parameter. Furthermore, we find that the phase factor in the ground state related to the system topology can be revealed by a real space correlation function. Numerical results demonstrate that this method works well in the presence of disordered perturbation, lattice defects, or when irregular boundaries condition are adopted. In addition, the results of the real space correlation function between two edges of the system directly reflect the existence of topological edge modes, verifying the BBC from the perspective of real-space bulk and edge correlations.

The conclusions in this paper, including the results of numerical simulations, reveal the consequence of the competition between the on-site and nearest neighbor pairings in a quadratic Hamiltonian and provide another real-space scheme for diagnosing the system topology.

ACKNOWLEDGMENTS

This work was supported by the National Natural Science Foundation of China (under Grant No. 12374461).

APPENDIX A: REAL SPACE CORRELATION

In this appendix, we present the method for computing the real space correlation function of the ground state of the quadratic Hamiltonian. We follow the method used in Ref. [55]. For simplicity, the system parameters are set to be uniform in real space, and the geometry is taken as an $N \times N$ square lattice. Other situations with disordered perturbations, random defects and irregular boundaries can be directly generalized.

Under the basis

$$C^\dagger = \left(c_{\mathbf{r}_{1,\downarrow}}^\dagger \cdots c_{\mathbf{r}_{N^2,\downarrow}}^\dagger, c_{\mathbf{r}_{1,\uparrow}}^\dagger, \cdots, c_{\mathbf{r}_{N^2,\uparrow}}^\dagger, \right. \\ \left. c_{\mathbf{r}_{1,\downarrow}} \cdots c_{\mathbf{r}_{N^2,\downarrow}}, c_{\mathbf{r}_{1,\uparrow}}, \cdots, c_{\mathbf{r}_{N^2,\uparrow}} \right), \quad (\text{A1})$$

the real space Hamiltonian in Eq. (1) can be written as

$$H = C^\dagger \tilde{H} C, \quad (\text{A2})$$

where \tilde{H} has the form

$$\tilde{H} = \begin{pmatrix} \mathbf{0} & M \\ -M & \mathbf{0} \end{pmatrix}, \quad (\text{A3})$$

and M is a $2N^2 \times 2N^2$ antisymmetric matrix. The

nonzero matrix elements are given in the following

$$\begin{aligned} M_{iN+j+N^2, (i-1)N+j} &= \frac{\Delta_+}{2}, \\ M_{(i-1)N+j+1+N^2, (i-1)N+j} &= \frac{\Delta_+}{2}, \\ M_{(i-1)N+j+N^2, iN+j} &= \frac{\Delta_-}{2}, \\ M_{(i-1)N+j+N^2, (i-1)N+j+1} &= \frac{\Delta_-}{2}, \\ M_{(i-1)N+j+N^2, (i-1)N+j} &= \frac{\Delta_0}{2}, \end{aligned} \quad (\text{A4})$$

where $i, j \in [1, N-1]$ and each corresponding transpose matrix element has a negative sign difference. By diagonalizing \tilde{H} , we have

$$\begin{aligned} H &= C^\dagger S \mathcal{E} S^T C \\ &= \Phi^\dagger \mathcal{E} \Phi \\ &= \sum_{m=1}^{N^2} \sum_{\sigma=\uparrow, \downarrow} \varepsilon_{m,\sigma} (\gamma_{m,\sigma}^\dagger \gamma_{m,\sigma} - \gamma_{m,\sigma} \gamma_{m,\sigma}^\dagger), \end{aligned} \quad (\text{A5})$$

where $\varepsilon_{m,\sigma} \geq 0$ and S is a real orthogonal matrix, which has the following form

$$S = \begin{pmatrix} \varphi & \chi \\ \chi & \varphi \end{pmatrix}, \quad (\text{A6})$$

due to the particle-hole symmetry of the BdG Hamiltonian. The columns of the matrix S are formed by the eigenvectors of \tilde{H} and φ and χ are both $2N^2 \times 2N^2$ matrices. The diagonal matrix \mathcal{E} has the form

$$\begin{aligned} \mathcal{E} &= S^T \tilde{H} S \\ &= \text{diag} (\varepsilon_{1,\downarrow}, \cdots, \varepsilon_{N^2,\downarrow}, \varepsilon_{1,\uparrow}, \cdots, \varepsilon_{N^2,\uparrow}, \\ &\quad -\varepsilon_{1,\downarrow}, \cdots, -\varepsilon_{N^2,\downarrow}, -\varepsilon_{1,\uparrow}, \cdots, -\varepsilon_{N^2,\uparrow}), \end{aligned} \quad (\text{A7})$$

and the new basis is

$$\begin{aligned} \Phi^\dagger &= C^\dagger S \\ &= \left(\gamma_{1,\downarrow}^\dagger, \cdots, \gamma_{N^2,\downarrow}^\dagger, \gamma_{1,\uparrow}^\dagger, \cdots, \gamma_{N^2,\uparrow}^\dagger, \right. \\ &\quad \left. \gamma_{1,\downarrow}, \cdots, \gamma_{N^2,\downarrow}, \gamma_{1,\uparrow}, \cdots, \gamma_{N^2,\uparrow} \right), \end{aligned} \quad (\text{A8})$$

where $\{\gamma_m^\dagger\}$ are fermionic operators, satisfying

$$\{\gamma_{m',\sigma'}, \gamma_{m,\sigma}^\dagger\} = \delta_{m',m} \delta_{\sigma',\sigma}, \{\gamma_{m',\sigma'}, \gamma_{m,\sigma}\} = 0. \quad (\text{A9})$$

Then the real space fermionic operators can be expressed as

$$\begin{aligned} c_{\mathbf{r}_{i,\downarrow}} &= \sum_{m=1}^{N^2} \left[\varphi_{i,m} \gamma_{m,\downarrow} + \varphi_{i,m+N^2} \gamma_{m,\uparrow} \right. \\ &\quad \left. + \chi_{i,m} \gamma_{m,\downarrow}^\dagger + \chi_{i,m+N^2} \gamma_{m,\uparrow}^\dagger \right], \end{aligned} \quad (\text{A10})$$

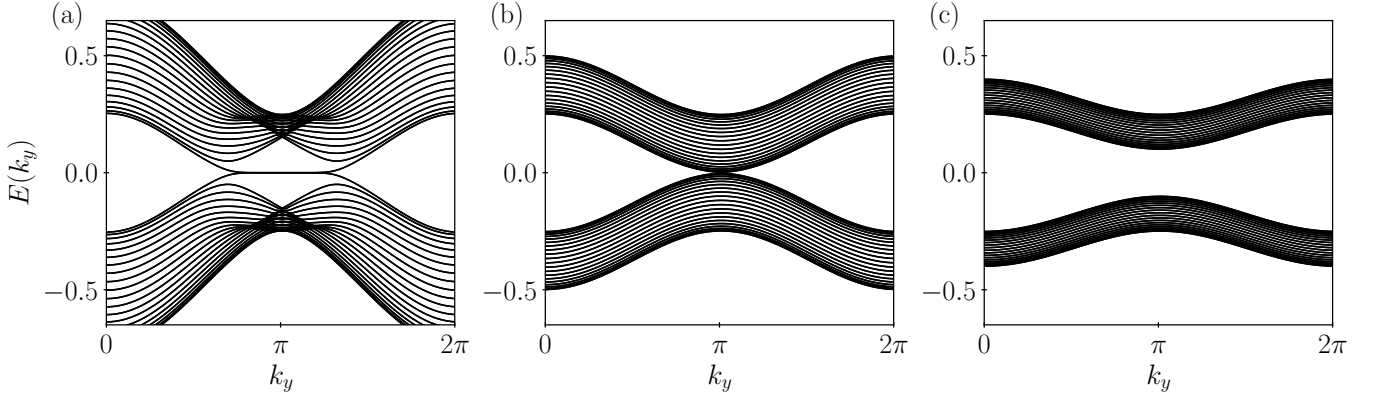


FIG. B1. Plots of the Majorana spectra of the Hamiltonian in Eq. (B5) with system size $N = 20$ for three typical cases with parameters taken the same as those in Figs. 3 (a)-(c): (a) topological nontrivial case $\Delta_+ = 0.8$, (b) critical case $\Delta_+ = 0.3$ and (c) topological trivial case $\Delta_+ = 0.1$. Other parameters are $\Delta_0 = 1$ and $\Delta_- = 0.2$. All the spectra are globally twofold degenerate.

and

$$c_{\mathbf{r}_i, \uparrow} = \sum_{m=1}^{N^2} [\varphi_{i+N^2, m} \gamma_{m, \downarrow} + \varphi_{i+N^2, m+N^2} \gamma_{m, \uparrow} + \chi_{i+N^2, m} \gamma_{m, \downarrow}^\dagger + \chi_{i+N^2, m+N^2} \gamma_{m, \uparrow}^\dagger]. \quad (\text{A11})$$

The ground state of the system has the form

$$|G\rangle = \prod_{m=1}^{N^2} \prod_{\sigma=\uparrow, \downarrow} \gamma_{m, \sigma} |0\rangle. \quad (\text{A12})$$

Taking the anticommutation relation of $\{\gamma_m^\dagger\}$ in Eq. (A8) and the form of the ground state $|G\rangle$ in Eq. (A12) into account, the real space correlation function can be computed as

$$\begin{aligned} & \langle G | c_{\mathbf{r}_j, \uparrow} c_{\mathbf{r}_i, \downarrow} | G \rangle \\ &= \sum_{m=1, n=1}^{N^2} \langle [\varphi_{j+N^2, m} \gamma_{m, \downarrow} + \varphi_{j+N^2, m+N^2} \gamma_{m, \uparrow}] \\ & \quad \times [\chi_{i, n} \gamma_{n, \downarrow}^\dagger + \chi_{i, n+N^2} \gamma_{n, \uparrow}^\dagger] \rangle \\ &= \sum_{m=1}^{2N^2} \varphi_{j+N^2, m} \chi_{i, m} \\ &= (\varphi \chi^T)_{j+N^2, i}, \end{aligned} \quad (\text{A13})$$

where φ and χ defined in Eq. (A6) are computed from the exact diagonalization of the Hamiltonian matrix \tilde{H} in Eq. (A3).

APPENDIX B: MAJORANA LATTICE AND EDGE MODES

To gain intuition on the edge modes, we introduce the Majorana fermion operators $a_{\mathbf{r}, \sigma} = c_{\mathbf{r}, \sigma}^\dagger + c_{\mathbf{r}, \sigma}$, $b_{\mathbf{r}, \sigma} =$

$-i(c_{\mathbf{r}, \sigma}^\dagger - c_{\mathbf{r}, \sigma})$, which satisfy the anticommutation relations $\{a_{\mathbf{r}, \sigma}, a_{\mathbf{r}', \sigma'}\} = 2\delta_{\mathbf{r}, \mathbf{r}'} \delta_{\sigma, \sigma'}$, $\{b_{\mathbf{r}, \sigma}, b_{\mathbf{r}', \sigma'}\} = 2\delta_{\mathbf{r}, \mathbf{r}'} \delta_{\sigma, \sigma'}$ and $\{a_{\mathbf{r}, \sigma}, b_{\mathbf{r}', \sigma'}\} = 0$. The Majorana representation of the real space Hamiltonian in Eq. (1) is

$$H = \sum_{\mathbf{r}} \sum_{\mathbf{a}=\hat{x}, \hat{y}} \Upsilon_{\mathbf{r}}^\dagger T_{\text{NN}} \Upsilon_{\mathbf{r}+\mathbf{a}} + \text{H.c.} + \sum_{\mathbf{r}} \Upsilon_{\mathbf{r}}^\dagger T_{\text{O}} \Upsilon_{\mathbf{r}}, \quad (\text{B1})$$

where $\Upsilon_{\mathbf{r}}^\dagger = (a_{\mathbf{r}, \uparrow} \ a_{\mathbf{r}, \downarrow} \ b_{\mathbf{r}, \uparrow} \ b_{\mathbf{r}, \downarrow})$, and the coefficient matrix for nearest neighbor and on-site pairing terms are

$$T_{\text{NN}} = \frac{1}{4} i \Delta_- (\sigma_x \otimes \sigma_+) - \frac{1}{4} i \Delta_+ (\sigma_x \otimes \sigma_-), \quad (\text{B2})$$

and

$$T_{\text{O}} = -\frac{1}{4} \Delta_0 (\sigma_x \otimes \sigma_y), \quad (\text{B3})$$

respectively, with $\sigma_{\pm} = (\sigma_x \pm \sigma_y)/2$.

Next, we consider the $N \times N$ square lattice with cylindrical boundaries condition: taking open boundary conditions in the x direction and periodic boundary condition in the y direction. Then, take the following Fourier transformations for the Majorana fermion operators:

$$\begin{pmatrix} a_{m, k_y, \sigma} \\ b_{m, k_y, \sigma} \end{pmatrix} = \frac{1}{\sqrt{N}} \sum_n e^{-ik_y n} \begin{pmatrix} a_{m, n, \sigma} \\ b_{m, n, \sigma} \end{pmatrix}, \quad (\text{B4})$$

where $k_y = 2\pi l/N$, with $l = 0, 1, \dots, N-1$. Note that in general, $a_{m, k_y, \sigma}$ and $b_{m, k_y, \sigma}$ are not Majorana fermion operators, except at $k_y = 0$ and π ; we refer to such operators as auxiliary operators. Then, the Hamiltonian can be written as $H = \sum_{k_y} H_{k_y}$, where

$$H_{k_y} = \sum_m \Upsilon_{m, k_y}^\dagger T_{\text{NN}}^{k_y} \Upsilon_{m+1, k_y} + \text{H.c.} + \sum_m \Upsilon_{m, k_y}^\dagger T_{\text{O}}^{k_y} \Upsilon_{m, k_y}, \quad (\text{B5})$$

with $\Upsilon_{m,k_y}^\dagger = (a_{m,k_y,\uparrow} \ a_{m,k_y,\downarrow} \ b_{m,k_y,\uparrow} \ b_{m,k_y,\downarrow})$, and

$$\begin{aligned} T_{\text{NN}}^{k_y} &= T_{\text{NN}}, \\ T_{\text{O}}^{k_y} &= i\eta_{k_y}^* (\sigma_x \otimes \sigma_+) - i\eta_{k_y} (\sigma_x \otimes \sigma_-), \\ \eta_{k_y} &= \frac{1}{4}(\Delta_+ e^{-ik_y} + \Delta_- e^{ik_y} + \Delta_0). \end{aligned} \quad (\text{B6})$$

We note that for each k_y , the Hamiltonian H_{k_y} represents a lattice of ladders about auxiliary operators $a_{m,k_y,\sigma}$ and $b_{m,k_y,\sigma}$. In Fig. B1, we show the numerical results of the single-particle spectra of H_{k_y} for three sets of typical parameters. We can see the existence of the flat-band zero modes in the topological nontrivial case in Fig. B1 (a).

Actually, in the large N limit, the Hamiltonian H_{k_y} is expected to possess zero energy edge modes, which can be determined by the following matrix equation

$$(T_{\text{NN}}^{k_y})^\dagger \Psi_{m-1,k_y} + T_{\text{O}}^{k_y} \Psi_{m,k_y} + T_{\text{NN}}^{k_y} \Psi_{m+1,k_y} = 0, \quad (\text{B7})$$

where $m = 1, 2, \dots, N$, and Ψ_{m,k_y} is a four-dimensional vector under the basis of Υ_{m,k_y} . The boundary condition is

$$\Psi_{0,k_y} = 0, \Psi_{N+1,k_y} = 0. \quad (\text{B8})$$

There are four zero energy edge modes when the winding number [12, 50–52] of the pseudo spin Hamiltonians $H(\mathbf{k})$ and $-H(-\mathbf{k})$ in Eq. (4)

$$\mathcal{W}_\pm(k_y) = \frac{1}{2\pi i} \int_{-\pi}^{\pi} dk_x \partial_{k_x} \ln[\pm g(\pm \mathbf{k})], \quad (\text{B9})$$

are nonzero, where $g(\mathbf{k}) = B_x(\mathbf{k}) + iB_y(\mathbf{k})$. It can be checked that the condition for $\mathcal{W}_\pm(k_y)$ to be nonzero is $|p_\pm| < 1$ and $|q_\pm| < 1$, where

$$\begin{aligned} p_\pm &= -\frac{2\eta_{k_y} \pm \sqrt{4\eta_{k_y}^2 - \Delta_+ \Delta_-}}{\Delta_+}, \\ q_\pm &= -\frac{2\eta_{k_y}^* \pm \sqrt{4(\eta_{k_y}^*)^2 - \Delta_+ \Delta_-}}{\Delta_-}. \end{aligned} \quad (\text{B10})$$

Under this condition, the zero modes are determined to be

$$\begin{aligned} \gamma_{k_y,\uparrow} &= A_\uparrow \sum_{j=1}^N \left[(p_+^j - p_-^j) a_{j,k_y,\uparrow} \right. \\ &\quad \left. + i(p_+^{N-j+1} - p_-^{N-j+1}) b_{j,k_y,\uparrow} \right], \end{aligned} \quad (\text{B11})$$

$$\begin{aligned} \gamma_{k_y,\downarrow} &= A_\downarrow \sum_{j=1}^N \left[(q_+^j - q_-^j) a_{j,k_y,\downarrow} \right. \\ &\quad \left. + i(q_+^{N-j+1} - q_-^{N-j+1}) b_{j,k_y,\downarrow} \right], \end{aligned} \quad (\text{B12})$$

and their corresponding Hermitian conjugate $\gamma_{k_y,\sigma}^\dagger$, in which A_σ is a normalization constant. It can be checked that the above edge zero mode operators are fermionic operators, since they satisfy the anticommutation relations

$$\begin{aligned} \{\gamma_{k_y,\sigma}, \gamma_{k'_y,\sigma'}^\dagger\} &= \delta_{k_y,k'_y} \delta_{\sigma,\sigma'}, \\ \{\gamma_{k_y,\sigma}, \gamma_{k'_y,\sigma'}\} &= 0. \end{aligned} \quad (\text{B13})$$

-
- [1] K. v. Klitzing, G. Dorda, and M. Pepper, New method for high-accuracy determination of the fine-structure constant based on quantized hall resistance, *Phys. Rev. Lett.* **45**, 494 (1980).
- [2] R. B. Laughlin, Quantized hall conductivity in two dimensions, *Phys. Rev. B* **23**, 5632 (1981).
- [3] D. J. Thouless, M. Kohmoto, M. P. Nightingale, and M. den Nijs, Quantized hall conductance in a two-dimensional periodic potential, *Phys. Rev. Lett.* **49**, 405 (1982).
- [4] R. B. Laughlin, Anomalous quantum hall effect: An incompressible quantum fluid with fractionally charged excitations, *Phys. Rev. Lett.* **50**, 1395 (1983).
- [5] F. D. M. Haldane, Model for a quantum hall effect without landau levels: Condensed-matter realization of the "parity anomaly", *Phys. Rev. Lett.* **61**, 2015 (1988).
- [6] C. L. Kane and E. J. Mele, Quantum spin hall effect in graphene, *Phys. Rev. Lett.* **95**, 226801 (2005).
- [7] M. König, S. Wiedmann, C. Brune, A. Roth, H. Buhmann, L. W. Molenkamp, X.-L. Qi, and S.-C. Zhang, Quantum spin hall insulator state in hgte quantum wells, *Science* **318**, 766 (2007).
- [8] L. Fu and C. L. Kane, Topological insulators with inversion symmetry, *Phys. Rev. B* **76**, 045302 (2007).
- [9] X.-L. Qi, T. L. Hughes, S. Raghu, and S.-C. Zhang, Time-reversal-invariant topological superconductors and superfluids in two and three dimensions, *Phys. Rev. Lett.* **102**, 187001 (2009).
- [10] X.-L. Qi and S.-C. Zhang, Topological insulators and superconductors, *Rev. Mod. Phys.* **83**, 1057 (2011).
- [11] C.-Z. Chang, J. Zhang, X. Feng, J. Shen, Z. Zhang, M. Guo, K. Li, Y. Ou, P. Wei, L.-L. Wang, *et al.*, Experimental observation of the quantum anomalous hall effect in a magnetic topological insulator, *Science* **340**, 167 (2013).
- [12] C. L. M. Wong, J. Liu, K. T. Law, and P. A. Lee, Majorana flat bands and unidirectional majorana edge states in gapless topological superconductors, *Phys. Rev. B* **88**, 060504 (2013).
- [13] C.-K. Chiu and A. P. Schnyder, Classification of reflection-symmetry-protected topological semimetals and nodal superconductors, *Phys. Rev. B* **90**, 205136 (2014).
- [14] F. Liu and K. Wakabayashi, Novel topological phase with a zero berry curvature, *Phys. Rev. Lett.* **118**, 076803 (2017).

- [15] T. Zhang, Y. Jiang, Z. Song, H. Huang, Y. He, Z. Fang, H. Weng, and C. Fang, Catalogue of topological electronic materials, *Nature* **566**, 475 (2019).
- [16] L. Xie, L. Jin, and Z. Song, Antihelical edge states in two-dimensional photonic topological metals, *Sci. Bull.* **68**, 255 (2023).
- [17] C.-K. Chiu, J. C. Y. Teo, A. P. Schnyder, and S. Ryu, Classification of topological quantum matter with symmetries, *Rev. Mod. Phys.* **88**, 035005 (2016).
- [18] A. P. Schnyder, S. Ryu, A. Furusaki, and A. W. W. Ludwig, Classification of topological insulators and superconductors in three spatial dimensions, *Phys. Rev. B* **78**, 195125 (2008).
- [19] B. Béri, Topologically stable gapless phases of time-reversal-invariant superconductors, *Phys. Rev. B* **81**, 134515 (2010).
- [20] R. Queiroz and A. P. Schnyder, Stability of flat-band edge states in topological superconductors without inversion center, *Phys. Rev. B* **89**, 054501 (2014).
- [21] A. P. Schnyder and P. M. Brydon, Topological surface states in nodal superconductors, *Journal of Physics: Condensed Matter* **27**, 243201 (2015).
- [22] A. Bouhon, J. Schmidt, and A. M. Black-Schaffer, Topological nodal superconducting phases and topological phase transition in the hyperhoneycomb lattice, *Phys. Rev. B* **97**, 104508 (2018).
- [23] S. Kobayashi, S. Sumita, Y. Yanase, and M. Sato, Symmetry-protected line nodes and majorana flat bands in nodal crystalline superconductors, *Phys. Rev. B* **97**, 180504 (2018).
- [24] A. K. Nayak, A. Steinbok, Y. Roet, J. Koo, G. Margalit, I. Feldman, A. Almoalem, A. Kanigel, G. A. Fiete, B. Yan, *et al.*, Evidence of topological boundary modes with topological nodal-point superconductivity, *Nature physics* **17**, 1413 (2021).
- [25] L. C. Xie, H. C. Wu, L. Jin, and Z. Song, Time-reversal symmetric topological metal, *Phys. Rev. B* **104**, 165422 (2021).
- [26] M. Bazarnik, R. Lo Conte, E. Mascot, K. von Bergmann, D. K. Morr, and R. Wiesendanger, Antiferromagnetism-driven two-dimensional topological nodal-point superconductivity, *Nature Communications* **14**, 614 (2023).
- [27] V. P. Mineev and K. V. Samokhin, *Introduction to unconventional superconductivity* (Gordon and Breach, New York, 1999).
- [28] L. P. Gor'kov and E. I. Rashba, Superconducting 2d system with lifted spin degeneracy: Mixed singlet-triplet state, *Phys. Rev. Lett.* **87**, 037004 (2001).
- [29] A. Aperis, G. Varelogiannis, P. Littlewood, and B. Simons, Coexistence of spin density wave, d-wave singlet and staggered π -triplet superconductivity, *Journal of Physics: Condensed Matter* **20**, 434235 (2008).
- [30] F. S. Bergeret and I. V. Tokatly, Singlet-triplet conversion and the long-range proximity effect in superconductor-ferromagnet structures with generic spin dependent fields, *Phys. Rev. Lett.* **110**, 117003 (2013).
- [31] G. Wang, T. Dvir, G. P. Mazur, C.-X. Liu, N. van Looy, S. L. Ten Haaf, A. Bordin, S. Gazibegovic, G. Badawy, E. P. Bakkers, *et al.*, Singlet and triplet cooper pair splitting in hybrid superconducting nanowires, *Nature* **612**, 448 (2022).
- [32] Y. Hatsugai, Chern number and edge states in the integer quantum hall effect, *Phys. Rev. Lett.* **71**, 3697 (1993).
- [33] J. Kellendonk, T. Richter, and H. Schulz-Baldes, Edge current channels and chern numbers in the integer quantum hall effect, *Reviews in Mathematical Physics* **14**, 87 (2002).
- [34] X.-L. Qi, Y.-S. Wu, and S.-C. Zhang, General theorem relating the bulk topological number to edge states in two-dimensional insulators, *Phys. Rev. B* **74**, 045125 (2006).
- [35] R. S. K. Mong and V. Shivamoggi, Edge states and the bulk-boundary correspondence in dirac hamiltonians, *Phys. Rev. B* **83**, 125109 (2011).
- [36] A. M. Essin and V. Gurarie, Bulk-boundary correspondence of topological insulators from their respective green's functions, *Phys. Rev. B* **84**, 125132 (2011).
- [37] R. Bianco and R. Resta, Mapping topological order in coordinate space, *Phys. Rev. B* **84**, 241106 (2011).
- [38] J. Sykes and R. Barnett, Local topological markers in odd dimensions, *Phys. Rev. B* **103**, 155134 (2021).
- [39] W. Chen, Optical absorption measurement of spin berry curvature and spin chern marker, *Journal of Physics: Condensed Matter* **35**, 155601 (2023).
- [40] W. Chen, Universal topological marker, *Phys. Rev. B* **107**, 045111 (2023).
- [41] Z. Ringel and Y. E. Kraus, Determining topological order from a local ground-state correlation function, *Phys. Rev. B* **83**, 245115 (2011).
- [42] L. Lepori, M. Burrello, A. Trombettoni, and S. Paganelli, Strange correlators for topological quantum systems from bulk-boundary correspondence, *Phys. Rev. B* **108**, 035110 (2023).
- [43] H. Li and F. D. M. Haldane, Entanglement spectrum as a generalization of entanglement entropy: Identification of topological order in non-abelian fractional quantum hall effect states, *Phys. Rev. Lett.* **101**, 010504 (2008).
- [44] A. M. Turner, Y. Zhang, and A. Vishwanath, Entanglement and inversion symmetry in topological insulators, *Phys. Rev. B* **82**, 241102 (2010).
- [45] E. Prodan, T. L. Hughes, and B. A. Bernevig, Entanglement spectrum of a disordered topological chern insulator, *Phys. Rev. Lett.* **105**, 115501 (2010).
- [46] J. Li, R.-L. Chu, J. K. Jain, and S.-Q. Shen, Topological anderson insulator, *Phys. Rev. Lett.* **102**, 136806 (2009).
- [47] Y.-Y. Zhang, R.-L. Chu, F.-C. Zhang, and S.-Q. Shen, Localization and mobility gap in the topological anderson insulator, *Phys. Rev. B* **85**, 035107 (2012).
- [48] E. J. Meier, F. A. An, A. Dauphin, M. Maffei, P. Massignan, T. L. Hughes, and B. Gadway, Observation of the topological anderson insulator in disordered atomic wires, *Science* **362**, 929 (2018).
- [49] J. Bardeen, L. N. Cooper, and J. R. Schrieffer, Theory of superconductivity, *Phys. Rev.* **108**, 1175 (1957).
- [50] S. Ryu and Y. Hatsugai, Topological origin of zero-energy edge states in particle-hole symmetric systems, *Phys. Rev. Lett.* **89**, 077002 (2002).
- [51] K. Sun, W. V. Liu, A. Hemmerich, and S. Das Sarma, Topological semimetal in a fermionic optical lattice, *Nature Physics* **8**, 67 (2012).
- [52] S. Matsuura, P.-Y. Chang, A. P. Schnyder, and S. Ryu, Protected boundary states in gapless topological phases, *New Journal of Physics* **15**, 065001 (2013).
- [53] Y. Wang, J.-J. Miao, H.-K. Jin, and S. Chen, Characterization of topological phases of dimerized kitaev chain via edge correlation functions, *Phys. Rev. B* **96**, 205428 (2017).
- [54] J.-J. Miao, H.-K. Jin, F.-C. Zhang, and Y. Zhou, Exact solution for the interacting kitaev chain at the symmetric

- point, [Phys. Rev. Lett. **118**, 267701 \(2017\)](#).
- [55] A. P. Young and H. Rieger, Numerical study of the random transverse-field ising spin chain, [Phys. Rev. B **53**, 8486 \(1996\)](#).